

# Condensed Matter and Interphases

Kondensirovannye Sredy i Mezhfaznye Granitsy  
<https://journals.vsu.ru/kcmf/>

## Original articles

Research article

<https://doi.org/10.17308/kcmf.2024.26/11819>

## Photoluminescent porous silicon nanowires as contrast agents for bioimaging

M. G. Shatskaia<sup>1</sup>, D. A. Nazarovskaia<sup>1</sup>, K. A. Gonchar<sup>1</sup>, Ya. V. Lomovskaya<sup>1,2</sup>, I. I. Tsiniiaikin<sup>1</sup>, O. A. Shalygina<sup>1</sup>, A. A. Kudryavtsev<sup>1,2,3</sup>, L. A. Osminkina<sup>1,3</sup>✉

<sup>1</sup>Lomonosov Moscow State University, Faculty of Physics,  
1 Leninskie Gory, Moscow 119991, Russian Federation

<sup>2</sup>Institute of Theoretical and Experimental Biophysics Russian Academy of Sciences,  
3 Institutskaya str., Pushchino 142290, Russian Federation

<sup>3</sup>Institute for Biological Instrumentation of the Russian Academy of Sciences,  
7 Institutskaya str., Pushchino 142290, Russian Federation

### Abstract

Porous silicon nanowires (pSi NWs) have attracted considerable interest due to their unique structural, optical properties and biocompatibility. The most common method for their top-down synthesis is metal-assisted chemical etching (MACE) of crystalline silicon (c-Si) wafers using silver nanoparticles as a catalyst. However, the replacement of silver with bioinert gold nanoparticles (Au NPs) markedly improves the efficiency of pSi NWs in biomedical applications. The present study demonstrates the fabrication of porous pSi NWs arrays using Au NPs as the catalyst in MACE of c-Si wafers with a resistivity of 1–5 mOhm-cm. Using scanning electron microscopy (SEM), the formation of arrays of porous nanowires with a diameter of 50 nm that consist of small silicon nanocrystals (nc-Si) and pores was observed. Raman spectroscopy analysis determined the size of nc-Si is about 4 nm. The pSi NWs exhibit effective photoluminescence (PL) with a peak in the red spectrum, which is attributed to the quantum confinement effect occurred in small 4 nm nc-Si. In addition, the pSi NWs exhibit low toxicity towards MCF-7 cancer cells, and their PL characteristics allow them to be used as contrast agents for bioimaging.

**Keywords:** Porous silicon nanowires, Photoluminescence, Raman spectroscopy, Contrast agents, Bioimaging

**Funding:** The study was supported by the Russian Science Foundation grant No. 22-72-10062, <https://rscf.ru/en/project/22-72-10062/> and the Theoretical Physics and Mathematics Advancement Foundation “BASIS” grant No. 23-2-2-18-1.

**Acknowledgements:** The equipment of the Educational and Methodological Centre for Lithography and Microscopy of Lomonosov Moscow State University was used in the study.

**For citation:** Shatskaia M. G., Nazarovskaia D. A., Gonchar K. A., Lomovskaya Ya. V., Tsiniiaikin I. I., Shalygina O. A., Kudryavtsev A. A., Osminkina L. A. Photoluminescent porous silicon nanowires as contrast agents for bioimaging. *Condensed Matter and Interphases*. 2024;26(1): 161–167. <https://doi.org/10.17308/kcmf.2024.26/11819>

**Для цитирования:** Шатская М. Г., Назаровская Д. А., Гончар К. А., Ломовская Я. В., Циньяйкин И. И., Шалыгина О. А., Кудрявцев А. А., Осминкина Л. А. Фотолуминесцентные пористые кремниевые нанонити как контрастные агенты для биовизуализации. *Конденсированные среды и межфазные границы*. 2024;26(1): 161–167. <https://doi.org/10.17308/kcmf.2024.26/11819>

✉ Liubov A. Osminkina, e-mail: [osminkina@physics.msu.ru](mailto:osminkina@physics.msu.ru)

© Shatskaia M. G., Nazarovskaia D. A., Gonchar K. A., Lomovskaya Ya. V., Tsiniiaikin I. I., Shalygina O. A., Kudryavtsev A. A., Osminkina L. A., 2024



The content is available under Creative Commons Attribution 4.0 License.

## 1. Introduction

Now, technologies for the design and use of nanomaterials in biomedicine are being intensively developed, and silicon nanowires and nanoparticles occupy a special place among them. It has been shown that silicon nanostructures can be used in a variety of fields: from drug delivery to tissue engineering [1]. This is possible due to such unique properties of nanostructured silicon as biocompatibility [2, 3], biodegradability [4, 5] and photoluminescence (PL) in the visible region of the spectrum [6,7]. PL is explained by the quantum confinement effect (QCE) in 2–6 nm silicon nanocrystals (nc-Si) [1, 4]. Due to the PL properties, porous silicon nanostructures have great potential in bioimaging [8–10]. In addition, the surface of porous silicon can be easily functionalized with silane groups, antibodies, polymers, etc., depending on the purpose [8, 11, 12].

There are several main methods for obtaining porous nanostructures on the surface of crystalline silicon substrates, and the most commonly used method is electrochemical (EC) etching [11, 13]. The result of EC etching of c-Si substrates is porous silicon (PSi) film, a spongy structure of nc-Si and pores. At the same time, by changing the parameters of the applied voltage, the level of c-Si doping and the concentration of electrolyte solutions used, macro-, meso-, and microporous films with pore sizes of 1–5 nm, 5–50 nm and 50–100 nm, respectively can be obtained [14]. The EC etching method is quite simple and easily scalable; however, mesoporous silicon films often used for biomedical purposes do not have sufficient PL properties for visualizing biological objects. The reason for this is that the nc-Si in them have too large size, far from the conditions for the occurrence of QCE. Therefore, to intensify the PL, PSi films or nanoparticles obtained from them are oxidized, thereby reducing the size of nc-Si, by incubating the samples in water, sodium tetraborate, or selecting drying conditions [8, 15, 16].

Metal-assisted chemical etching (MACE) of c-Si substrates is also the most commonly used method for producing silicon nanostructures [17]. Silver nanoparticles are usually used as a catalyst in MACE [18–20]. The result of MACE is arrays of silicon nanowires (SiNWs) with a diameter

of 20–100 nm on the c-Si surface. It has been shown that the porosity of SiNWs depends on the doping level of c-Si: the etching of low-doped substrates results in non-porous SiNWs, while the etching of highly doped substrates leads to the synthesis of porous SiNWs [18, 19, 21]. Porous SiNWs, immediately after their preparation, are characterized by mesoporous structure and effective stable PL, which undoubtedly facilitates the preparation of samples for potential use in the theranostics of diseases [22]. It should be noted, however, that there are no studies where PL of SiNWs synthesized by MACE with gold nanoparticles (Au NPs) would be investigated. It should be noted that the use of bioinert Au NPs can significantly improve the characteristics of SiNWs for their biomedical applications.

The purposes of the presented study were to obtain and investigate the morphology and PL properties of porous SiNWs synthesized using Au NPs as catalysts in MACE, and to show their use as contrast agents for the bioimaging of living cells.

## 2. Experimental

Porous SiNWs (pSi NWs) were synthesized by MACE of c-Si (100) substrates with a resistivity of 1–5 mOhm·cm. At the preliminary stage, c-Si was washed in acetone and isopropanol in an ultrasonic bath (Elmasonic US bath 37 KHz) for 5 min, then washed with deionized water (Millipore) and dried in air. To remove the oxide layer, the c-Si substrate was kept in 5 M HF for 2–5 min, then washed again with water and dried. Gold nanoparticles were reduced on the c-Si surface from an aqueous solution of 0.01 M AuCl<sub>3</sub>, mixed with 5 M HF in a ratio of 1:1, for 15 s. Silicon etching was performed in a solution of 5 M HF and 30% H<sub>2</sub>O<sub>2</sub> (10:1) for 60 min, the process was stopped by moving the wafers into water. Next, the samples were dried at room temperature in air. Removal of Au NPs was carried out by immersing the samples in aqua regia for 3 min.

To study the morphology of the obtained pSi NWs, a Carl Zeiss ULTRA 55 FE-SEM scanning electron microscope was used. To measure the PL or Raman spectra, the pSi NWs were mechanically separated from the c-Si substrate and placed on a metal substrate. Raman spectra were measured using a Confotec™ MR350 confocal microscope with laser excitation at 633 nm and low power of

1 mW to protect the samples from overheating. The PL spectra of the samples were measured upon excitation by a He-Cd laser at a wavelength of 325 nm (power of 10 mW, spot diameter of 1 mm). The PL signal was recorded using a grating monochromator (MS750, SOLAR TII) equipped with a CCD matrix.

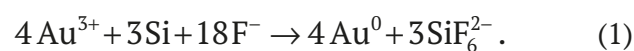
To study the cytotoxicity of pSi NWs, human ductal adenocarcinoma cell line MCF-7 was used. Cells were grown for 2 days in a culture flask with an area of 25 cm<sup>2</sup> in DMEM culture medium with the addition of 5% fetal bovine serum at 37 °C, 5% CO<sub>2</sub>. For the experiment, 0.1 ml of cell suspension with an initial cell concentration of 10<sup>5</sup>/ml was transferred into a 96-well plate. Then, pSi NWs with different concentrations were added to the wells, for which pSi NWs were mechanically separated from the c-Si substrates, the resulting powder was weighed and placed in a phosphate buffered saline solution. To determine the number of viable cells after a 24 h incubation with pSi NWs, the Alamar Blue test was performed: resazurin with a concentration of 0.03 mg/ml was added to the wells; living cells were able to oxidize it into luminescent resorufin. Luminescence intensity was recorded using an Infinite F200 plate spectrofluorimeter (Tecan).

For the biovisualization of cells with pSi NWs, a Leica confocal fluorescence microscope with a 63/NA 1.40 oil immersion objective and PL excitation with a 405 nm laser was used. pSi NWs with a concentration of 0.2 mg/ml were incubated with MCF-7 cells for 9 h before the start of the experiment. The cells were then stained by adding 3 mg/ml calcein-AM, Sigma for cytoplasmic

staining, and 5 mg/ml bisbenzimidazole H 33342 (Hoechst, Calbiochem) for nuclear staining.

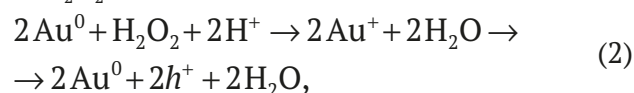
### 3. Results and discussion

Figure 1 shows a diagram of the production of pSi NWs using gold-assisted chemical etching (GACE) of highly doped c-Si wafers. At the first stage GACE, gold nanoparticles (Au NPs) were deposited from a solution of 0.01 M gold (III) chloride and 5 M HF, which dissociates in water into individual cations and anions and participates in the process of electrochemical reduction of Au<sup>3+</sup> ions into the metallic state on c-Si substrates [23]:

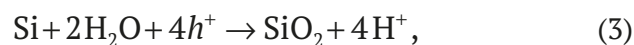


At the second stage of GACE, chemical etching of the c-Si substrate coated with Au NPs occurs in a solution of 5 M HF and 30% H<sub>2</sub>O<sub>2</sub> according to two parallel processes [18, 24].

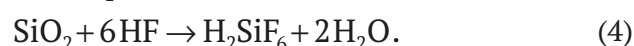
Au NPs (cathode site) catalyze the reduction of H<sub>2</sub>O<sub>2</sub>:



injected holes oxidize Si (anode site) to SiO<sub>2</sub>:



the SiO<sub>2</sub> layer is etched by hydrofluoric acid:



As a result of the presented redox reactions catalyzed by Au NPs, the c-Si surface is etched, and the remaining unetched areas have a nanowire-like morphology. Individual pSi NWs

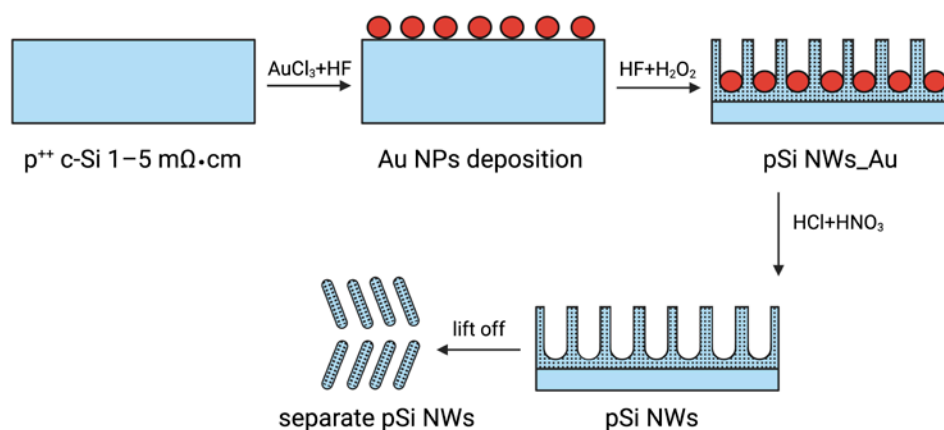


**Fig. 1.** Scheme for obtaining pSi NWs by gold-assisted chemical etching of highly doped c-Si wafers.

were obtained by mechanical separation from the c-Si substrate using tweezers.

The SEM micrograph of a cross-sectional view of porous pSi NWs on c-Si after 60 minutes of GACE is shown in Fig. 2a. pSi NWs appear as quasi-ordered arrays with a preferred orientation along the [100] crystallographic direction.

The pSi NWs layer thickness is 20  $\mu\text{m}$ . The tops of the pSi NWs stick together when they were dried due to capillary forces. The pore formation of pSi NWs was catalyzed by Au ions in the etching solution [18]. At the same time, the enlarged image (Fig. 2a) shows that the average diameter of the nanowires was 50 nm, and the pSi NWs consisted of small nanocrystals and pores. Micrographs of individual porous pSi NWs after their mechanical separation from the c-Si substrate are shown in Fig. 2b. The nanowires can break during the separation process; the average length of the obtained pSi NWs is 8  $\mu\text{m}$ .

The Raman spectrum (RS) of the obtained pSi NWs is shown in Fig. 3. Here, a scattering line characteristic of nanocrystalline silicon was observed with the position of the maximum shifted by  $\Delta\omega$  relative to 520.5  $\text{cm}^{-1}$ , corresponding to longitudinal vibrations of optical phonons in c-Si (shown by the dashed line). Such a low-frequency Raman shift occurs due to the quantum confinement of phonons arising in small-sized nc-Si contained in pSi NWs, their diameter ( $d_{RS}$ ) can be calculated using the formula [25, 4]:

$$d_{RS} = 0.543 \left( \frac{52.3}{\Delta\omega} \right)^{0.63}. \quad (5)$$

The nc-Si sizes calculated from formula (5) is 4.5 nm.

Using the MagicPlot package, deconvolution of the RS was obtained by Lorentian and Gaussian, responsible for the crystalline and amorphous phases in nc-Si, respectively. The percentage of crystalline silicon in porous SiNWs samples calculated in this way was 46.7%, and the percentage of amorphous silicon was 53.3%.

The PL spectrum of pSi NWs, represented by the wide band with a maximum at 755 nm is shown in Fig. 4. Such effective PL of pSi NWs was possible due to quantum confinement effects (QCE) arising in the nc-Si inside pSi NWs upon photoexcitation. QCE consists of secondary quantization of the energy of charge carriers of both electrons and holes in a quantum dot, nc-Si, which leads to an increase in the effective band gap [13]. This energy corresponds to the energy of emitted photons by photoluminescent nc-Si in such a way that the position of the maximum of the PL spectrum,  $E_{PL}$  related to the average size of nc-Si ( $d_{PL}$ ) in accordance with the empirical formula [7]:

$$E_{PL} = E_0 + \frac{3.73}{d_{PL}^{1.39}}, \quad (6)$$

Where  $E_0$  is the band gap in c-Si. From here an expression for the calculation of  $d_{PL}$  can be obtained:

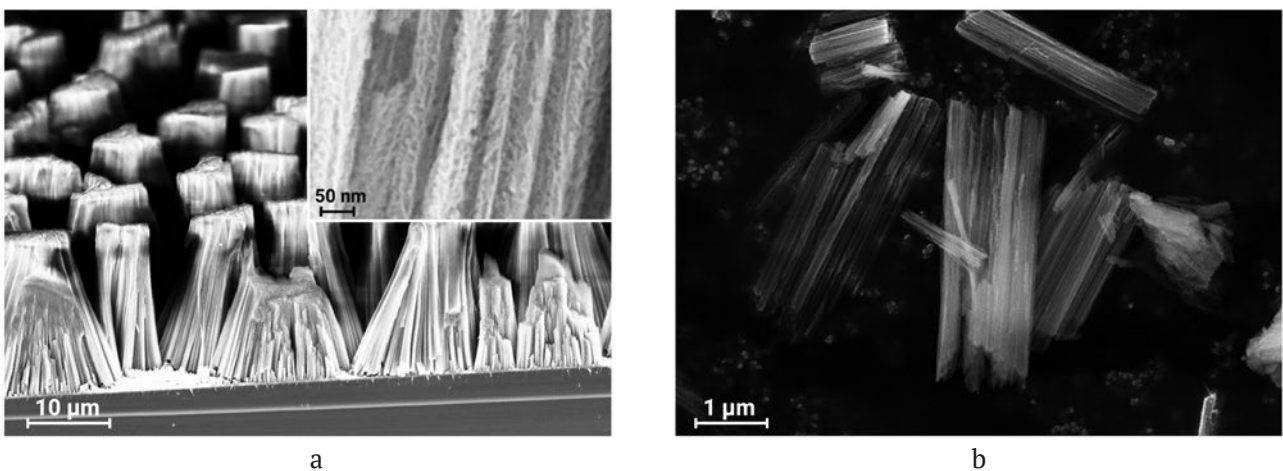


**Fig. 2.** SEM micrographs of pSi NWs, side view at an angle of 38° (a); and individual pSi NWs after their separation from the c-Si substrate (b). The inset in (a) shows an enlarged fragment of pSi NWs, demonstrating their porous structure

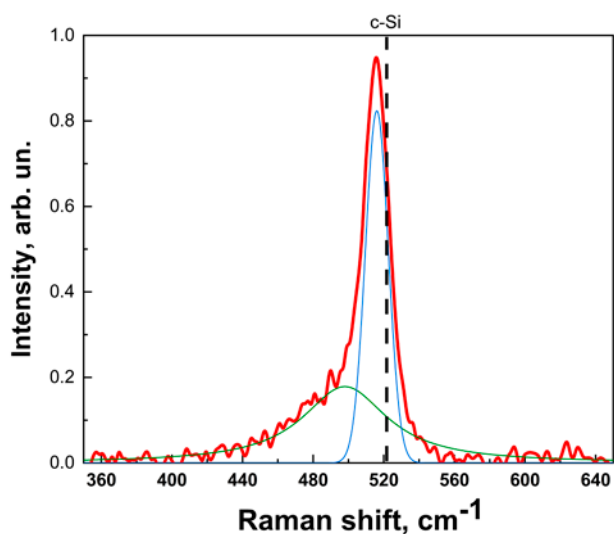


**Fig. 3.** Raman spectrum of pSi NWs. Thin lines represent the deconvolution of the spectrum. The dashed vertical line shows the position of the c-Si Raman maximum on  $520.5 \text{ cm}^{-1}$

$$d_{PL} = \left( \frac{3.73}{\Delta E_g} \right)^{0.72}, \quad (7)$$

where  $\Delta E_g = E_{PL} - E_0$ . The average size of nc-Si calculated using formula (7) is 4 nm, which is in good agreement with the Raman data.

The result of measuring the cytotoxicity of pSi NWs after 24 h incubation with MCF-7 cells is shown in Fig. 5. All points were taken in relation to the control group, to which pSi NWs was not added. It can be seen that over the entire range of concentrations studied, pSi NWs

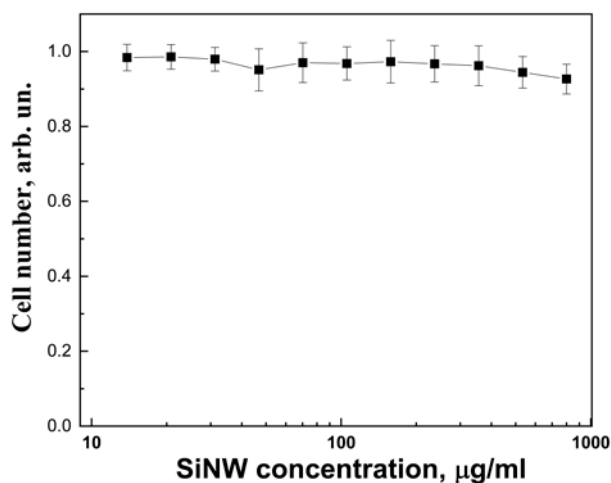


**Fig. 5.** Cytotoxicity of pSi NWs incubated for 24 h with MCF-7 cells. All points were taken in relation to the control group, to which pSi NWs was not added

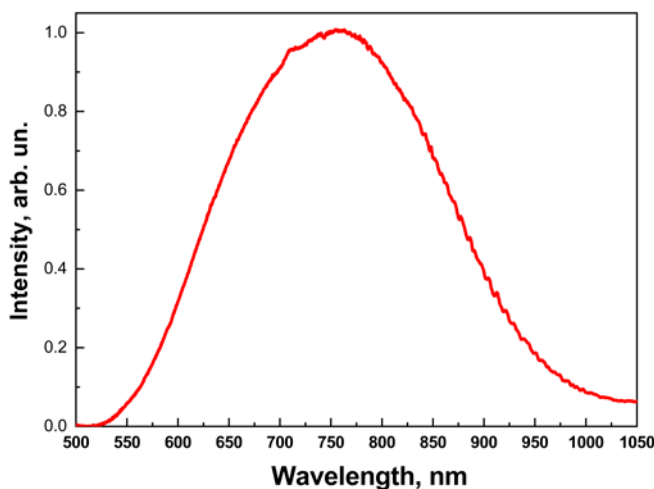


**Fig. 4.** PL spectrum of pSi NWs.

were characterized by extremely low toxicity, which is certainly a good result for their future applications in biomedicine.

Luminescent images of live MCF-7 cells after 9 h incubation with pSi NWs are shown in Fig. 6. Green, blue, and red colors correspond to the luminescence of the cell membrane, cell nucleus, and PL of pSi NWs, respectively. The merged image of cells with pSi NWs is shown in the lower right corner. In the presented micrograph, pSi NWs are visible as PL red thread-like structures located on the membrane and inside the cells. Thus, it has been shown that low-toxic PL pSi

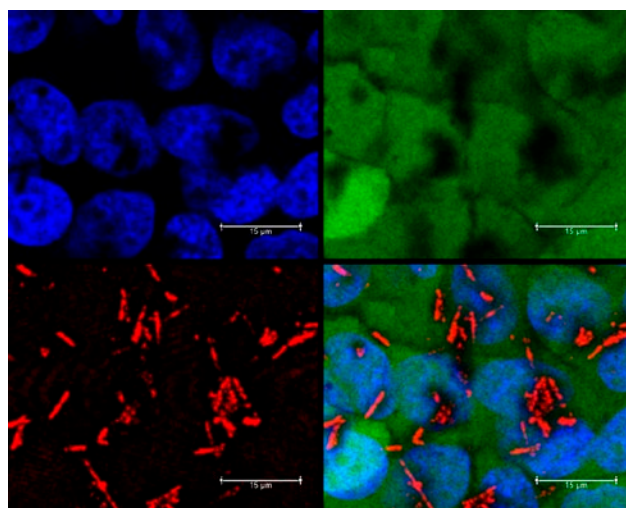


**Fig. 6.** Luminescence images of live MCF-7 cells after 9 h of incubation with pSi NWs. Green, blue, and red colors correspond to the luminescence of the cell membrane, cell nucleus, and PL of pSi NWs, respectively. The lower right corner shows a merged image of cells with pSi NWs.

NWs can be used as contrast agents for cell bioimaging.

#### 4. Conclusions

In this study, pSi NWs arrays were obtained by the GACE method, where Au NPs were used as a catalyst. The morphology of the samples was studied by scanning electron microscopy. It has been shown that GACE of c-Si wafers with a resistivity of 1–5 mOhm-cm produced arrays of porous nanowires with the diameter of 50 nm consisting of nc-Si and pores. The size of nc-Si was calculated based on the Raman spectra of pSi NWs and was about 4.5 nm. It was shown that, due to the quantum confinement effect, effective PL with a maximum in the red region of the spectrum can be excited in such pSi NWs. In this case, the size of nc-Si, calculated from the PL spectra of pSi NWs, was about 4 nm, which is in good agreement with the Raman data. It has been shown that pSi NWs were characterized by low toxicity towards MCF-7 cancer cells up to concentrations of 1 mg/ml, and the PL properties of pSi NWs allow their use as contrast agents for bioimaging. The presented data open up new possibilities for the use of low-toxic PL pSi NWs for theranostics of various diseases.

#### Contribution of the authors

The authors contributed equally to this article.

#### Conflict of interests

The authors declare that they have no known competing financial interests or personal relationships that could have influenced the work reported in this paper.

#### References

1. Canham L. (Ed.). *Handbook of porous silicon*. Berlin, Germany: Springer International Publishing; 2018. <https://doi.org/10.1007/978-3-319-71381-6>
2. Canham L. T. Nanoscale semiconducting silicon as a nutritional food additive. *Nanotechnology*. 2007;18: 185704. <https://dx.doi.org/10.1088/0957-4484/18/18/185704>
3. Low S. P., Voelcker N. H., Canham L. T., Williams K. A. The biocompatibility of porous silicon in tissues of the eye. *Biomaterials*. 2009;30: 2873–2880. <https://doi.org/10.1016/j.biomaterials.2009.02.008>
4. Gongalsky M. B., Tsurikova U. A., Gonchar K. A., Gvindgiiiiia G. Z., Osminkina L. A. Quantum-confinement effect in silicon nanocrystals during their dissolution in model biological fluids. *Semiconductors*. 2021;55(1): 61–65. <https://doi.org/10.1134/s1063782621010097>
5. Maximchik P. V., Tamarov K., Sheval E. V., ... Osminkina L. A. Biodegradable porous silicon nanocontainers as an effective drug carrier for regulation of the tumor cell death pathways. *ACS Biomaterials Science & Engineering*. 2019;5(11): 6063–6071. <https://doi.org/10.1021/acsbiomaterials.9b01292>
6. Delerue C., Allan G., Lannoo M. Theoretical aspects of the luminescence of porous silicon. *Physical Review B*. 1993;48: 11024. <https://doi.org/10.1103/PhysRevB.48.11024>
7. Ledoux G., Guillois O., Porterat D., ... Pillard V. Photoluminescence properties of silicon nanocrystals as a function of their size. *Physical Review B*. 2000;62: 15942. <https://doi.org/10.1103/PhysRevB.62.15942>
8. Park J. H., Gu L., von Maltzahn G., Ruoslahti E., Bhatia S. N., Sailor M. J. Biodegradable luminescent porous silicon nanoparticles for in vivo applications. *Nature Materials*. 2009;8: 331–336. <https://doi.org/10.1038/nmat2398>
9. Tolstik E., Gongalsky M. B., Dierks J., ... Lorenz K. Raman and fluorescence microspectroscopy applied for the monitoring of sunitinib-loaded porous silicon nanocontainers in cardiac cells. *Frontiers in Pharmacology*. 2022;13: 962763. <https://doi.org/10.3389/fphar.2022.962763>
10. Gu L., Hall D. J., Qin Z., ... Sailor M. J. In vivo time-gated fluorescence imaging with biodegradable luminescent porous silicon nanoparticles. *Nature Communications*. 2003;4: 2326. <https://doi.org/10.1038/ncomms3326>
11. Salonen J., Lehto V. P. Fabrication and chemical surface modification of mesoporous silicon for biomedical applications. *Chemical Engineering Journal*. 2008;137: 162–172. <https://doi.org/10.1016/j.cej.2007.09.001>
12. Gongalsky M. B., Kharin A. Y., Osminkina L. A., ... Chung B. H. Enhanced photoluminescence of porous silicon nanoparticles coated by bioresorbable polymers. *Nanoscale Research Letters*. 2012;7: 1–7. <https://doi.org/10.1186/1556-276X-7-446>
13. Canham L. T. Silicon quantum wire array fabrication by electrochemical and chemical dissolution of wafers. *Applied Physics Letters*. 1990;57: 1046–1048. <https://doi.org/10.1063/1.103561>
14. Lehmann V., Stengl R., Luigart A. On the morphology and the electrochemical formation mechanism of mesoporous silicon. *Materials Science and Engineering: B*. 2000;69: 11–22. [https://doi.org/10.1016/S0921-5107\(99\)00286-X](https://doi.org/10.1016/S0921-5107(99)00286-X)
15. Gongalsky M. B., Kargina J. V., Cruz J. F., ... Sailor M. J. Formation of Si/SiO<sub>2</sub> Luminescent quantum dots from mesoporous silicon by sodium tetraborate/

citric acid oxidation treatment. *Frontiers in Chemistry*. 2019;7: 165. <https://doi.org/10.3389/fchem.2019.00165>

16. Titova S. S., Osminkina L. A., Kakuliia ... Turishchev S. Y. X-ray photoelectron spectroscopy of hybrid 3T3 NIH cell structures with internalized porous silicon nanoparticles on substrates of various materials. *Condensed Matter and Interphases*. 2023;25(1): 132–138. <https://doi.org/10.17308/kcmf.2023.25/10983>

17. Peng K. Q., Hu J. J., Yan Y. J., ... Zhu J. Fabrication of single-crystalline silicon nanowires by scratching a silicon surface with catalytic metal particles. *Advanced Functional Materials*. 2006;16(3): 387–394. <https://doi.org/10.1002/adfm.200500392>

18. Chiappini C., Liu X., Fakhoury J. R., Ferrari M. Biodegradable porous silicon barcode nanowires with defined geometry. *Advanced Functional Materials*. 2010;20(14): 2231–2239. <https://doi.org/10.1002/adfm.201000360>

19. Turishchev S. Yu., Terekhov V. A., Nesterov D. N. ... Domashevskaya E. P. Electronic structure of silicon nanowires formed by MAWCE method. *Condensed Matter and Interphases*. . 2016;18(1): 130–141. Available at: <http://https://journals.vsu.ru/kcmf/article/view/117>

20. Gonchar K. A., Zubairova A. A., Schleusener A., Osminkina L. A., Sivakov V. Optical properties of silicon nanowires fabricated by environment-friendly chemistry. *Nanoscale Research Letters*. 2016;11: 1–5. <https://doi.org/10.1186/s11671-016-1568-5>

21. Tolstik E., Osminkina L. A., Akimov D., ... Popp J. Linear and non-linear optical imaging of cancer cells with silicon nanoparticles. *International Journal of Molecular Sciences*. 2016;17(9): 1536. <https://doi.org/10.3390/ijms17091536>

22. Osminkina L. A., Sivakov V. A., Mysov G. A., ... Timoshenko V. Yu. Nanoparticles prepared from porous silicon nanowires for bio-imaging and sonodynamic therapy. *Nanoscale Research Letters*. 2014; 9: 463. <https://doi.org/10.1186/1556-276X-9-463>

23. Osminkina L. A., Žukovskaja O., Agafilushkina S. N., ... Sivakov V. Gold nanoflowers grown in a porous Si/SiO<sub>2</sub> matrix: The fabrication process and plasmonic properties. *Applied Surface Science*. 2020;507: 144989. <https://doi.org/10.1016/j.apsusc.2019.144989>

24. Akan R., Parfeniukas K., Vogt C., Toprak M. S., Vogt, U. Reaction control of metal-assisted chemical etching for silicon-based zone plate nanostructures. *RSC Advances*. 2018;8(23): 12628–12634. <https://doi.org/10.1039/C8RA01627E>

25. Zi J., Zhang K., Xie X. Comparison of models for Raman spectra of Si nanocrystals. *Physical Review B*. 1997;55(15): 9263. <https://doi.org/10.1103/PhysRevB.55.9263>

## Information about authors

*Maria G. Shatskaia*, student, Faculty of Physics, Lomonosov Moscow State University (Moscow, Russian Federation).

[shatskaia.mg19@physics.msu.ru](mailto:shatskaia.mg19@physics.msu.ru)

*Daria A. Nazarovskaia*, graduate student, Faculty of Physics, Lomonosov Moscow State University (Moscow, Russian Federation).

<https://orcid.org/0000-0001-8151-9602>

[nazarovskaia.da22@physics.msu.ru](mailto:nazarovskaia.da22@physics.msu.ru)

*Kirill A., Gonchar*, Cand. Sci. (Phys.–Math.), Researcher, Faculty of Physics, Lomonosov Moscow State University (Moscow, Russian Federation).

<https://orcid.org/0000-0002-2301-2886>

[k.a.gonchar@gmail.com](mailto:k.a.gonchar@gmail.com)

*Yana V. Lomovskaya*, graduate student, Institute of Theoretical and Experimental Biophysics Russian Academy of Sciences (Pushchino, Russian Federation).

[yannalomovskaya@gmail.com](mailto:yannalomovskaya@gmail.com)

*Iliia I. Tsiniiaikin*, graduate student, Faculty of Physics Lomonosov Moscow State University (Moscow, Russian Federation).

<https://orcid.org/0000-0002-5820-8774>

[ii.tcinyaykin@physics.msu.ru](mailto:ii.tcinyaykin@physics.msu.ru)

*Olga A. Shalygina*, Cand. Sci. (Phys.–Math.), Associate Professor, Faculty of Physics, Lomonosov Moscow State University (Moscow, Russian Federation).

<https://orcid.org/0000-0002-0067-318X>

[shalygina@physics.msu.ru](mailto:shalygina@physics.msu.ru)

*Andrey A. Kudryavtsev*, Cand. Sci. (Phys.–Math.), Leading Researcher, Institute of Theoretical and Experimental Biophysics Russian Academy of Sciences, Institute for Biological Instrumentation of the Russian Academy of Sciences (Pushchino, Russian Federation).

[centavr42@mail.ru](mailto:centavr42@mail.ru)

*Liubov A. Osminkina*, Cand. Sci. (Phys.–Math.), Leading Researcher, Faculty of Physics, Moscow Lomonosov Moscow State University (Moscow, Russian Federation), Institute for Biological Instrumentation of the Russian Academy of Sciences (Pushchino, Russian Federation).

<https://orcid.org/0000-0001-7485-0495>

[osminkina@physics.msu.ru](mailto:osminkina@physics.msu.ru)

Received 19.04.2023; approved after reviewing 28.04.2023; accepted for publication 10.05.2023; published online 25.03.2024.

Translated by Valentina Mittova